

Magnetic structures produced by the small-scale dynamo

S. Louise Wilkin, Carlo F. Barenghi, and Anvar Shukurov

School of Mathematics and Statistics, Newcastle University, Newcastle upon Tyne, NE1 7RU, UK

(Dated: June 22, 2021)

Small-scale dynamo action has been obtained for a flow previously used to model fluid turbulence, where the sensitivity of the magnetic field parameters to the kinetic energy spectrum can be explored. We apply quantitative morphology diagnostics, based on the Minkowski functionals, to magnetic fields produced by the kinematic small-scale dynamo to show that magnetic structures are predominantly filamentary rather than sheet-like. Our results suggest that the thickness, width and length of the structures scale differently with magnetic Reynolds number as $R_m^{-2/(1-s)}$ and $R_m^{-0.55}$ for the former two, whereas the latter is independent of R_m , with s the slope of the energy spectrum.

PACS numbers: 47.65.-d, 07.55.Db, 02.40.Pc

The fluctuation (or small-scale) dynamo is a turbulent dynamo mechanism where a random flow of electrically conducting fluid generates a random magnetic field with zero mean value (the other type of dynamo relies on deviations of the flow from mirror symmetry, and perhaps other symmetries, and produces mean magnetic fields). This dynamo mechanism appears to be responsible for the random magnetic fields in the interstellar medium [1] and in galaxy clusters [2, 3, 4]. A necessary condition for the small-scale dynamo is that the magnetic Reynolds number R_m is large enough that the random velocity shear dominates over the effects of the fluid's electric resistivity. Here $R_m = ul/\eta$ where u and l are a typical velocity and length-scale respectively and η is the magnetic diffusivity. The critical magnetic Reynolds number, $R_{m,cr}$, is 30–500, depending on the nature of the flow [5, 6, 7, 9, 10, 11]. Numerical simulations of the non-linear, saturated states of the small-scale dynamo have been reviewed in ref. [11], but more insight can be gained by a careful analysis of the kinematic regime where the magnetic field is still too weak to affect the flow. In particular, the turbulent inertial range is undeveloped for the modest values of the Reynolds number achievable in direct numerical simulations; therefore, numerical results are often ambiguous.

Here we study the kinematic small-scale dynamo by solving numerically the induction equation

$$\frac{\partial \mathbf{B}}{\partial t} = \nabla \times (\mathbf{u} \times \mathbf{B}) + \eta \nabla^2 \mathbf{B}, \quad \nabla \cdot \mathbf{B} = 0, \quad (1)$$

for the magnetic field \mathbf{B} in a prescribed flow $\mathbf{u}(\mathbf{x}, t)$. Unlike other numerical models of the small-scale dynamo, our choice of the velocity field allows us to control fully its energy spectrum and time variation. In particular, the flow has a well pronounced power-law spectral range with controllable spectral slope. We use a spectral model for \mathbf{u} , specified in Eq. (2), which was developed as a Lagrangian model of turbulence and contains its essential features: it is three dimensional, time-dependent, multi-scale and has transport properties (two-particle dispersion, etc.) which agree remarkably well with those of tur-

bulent flows [13, 14] in both experiments and numerical calculations. Therefore, our main results are comparable with numerical experiments [16, 17] and to some extent with experimental results [15]. The velocity field \mathbf{u} is given by

$$\mathbf{u}(\mathbf{x}, t) = \sum_{n=1}^N \left[\mathbf{C}_n \times \hat{\mathbf{k}}_n \cos \phi_n + \mathbf{D}_n \times \hat{\mathbf{k}}_n \sin \phi_n \right], \quad (2)$$

where $\phi_n = \mathbf{k}_n \cdot \mathbf{x} + \omega_n t$, N is the number of modes and $\hat{\mathbf{k}}_n$ are randomly chosen unit vectors ($\mathbf{k}_n = k_n \hat{\mathbf{k}}_n$ is the wave vector); note that \mathbf{u} is solenoidal by construction. The directions of \mathbf{C}_n and \mathbf{D}_n are chosen randomly; we require, however, that they are normal to \mathbf{k}_n , so that the root mean velocity of each mode is $[(C_n^2 + D_n^2)/2]^{1/2}$. The magnitudes of \mathbf{C}_n and \mathbf{D}_n are chosen to reproduce the desired energy spectrum, $E(k)$: $C_n = D_n = [\frac{2}{3}E(k_n)\Delta k_n]^{1/2}$, where $\Delta k_n = \frac{1}{2}(k_{n+1} - k_{n-1})$ for $2 \leq n \leq N-1$, but $\Delta k_1 = \frac{1}{2}(k_2 - k_1)$ and $\Delta k_N = \frac{1}{2}(k_N - k_{N-1})$. For example, a model spectrum with suitable behaviors at $k \rightarrow 0$, $k \rightarrow \infty$, and $E(k) \propto k^s$ within the inertial range $k_0 \ll k \ll k_d$, can be implemented with

$$E(k) = ak_n^4 \left[1 + \left(\frac{k_n}{k_0} \right)^2 \right]^{(s-4)/2} \exp \left[-\frac{1}{2} \left(\frac{k_n}{k_d} \right)^2 \right], \quad (3)$$

where k_0 is the integral scale of the flow, k_d is the dissipation wavenumber and a is the normalization constant used to control the intensity of the flow. The Kolmogorov inertial range spectrum is obtained for $s = -5/3$. The frequencies $\omega_n = [k_n^3 E(k_n)]^{1/2}$ introduce time variation such that each mode varies at its ‘eddy turnover’ time.

Having specified k_0 and k_d , we can introduce the effective Reynolds number via $Re = (k_d/k_0)^{(1-s)/2}$ and $R_m = \langle u^2 \rangle^{1/2} l_0 / \eta$ for the magnetic Reynolds number, where angular brackets denote suitable averaging and $l_0 = 2\pi/k_0$. We enforce periodicity in the unit box by choosing \mathbf{k}_n randomly from a family of vectors whose components are multiples of 2π . The resulting kinetic energy spectrum $E(k)$ for $s = -5/3$ is shown in Fig. 1 (solid line), defined as $\int_0^\infty E(k) dk = V^{-1} \int_V \frac{1}{2} |\mathbf{u}|^2 dV$,

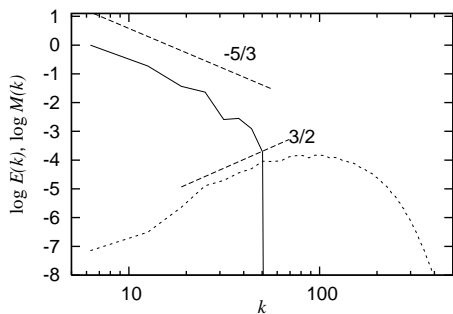


FIG. 1: Typical energy spectra for the velocity field (E , solid) and a growing magnetic field (M , dotted) in arbitrary units, with $N = 40$, $k_0 = 2\pi$ and $k_d \approx 16\pi$; this corresponds to the effective Reynolds number $\text{Re} \approx 16$ and $R_m \approx 2000$. Dashed lines represent power laws with the slopes indicated.

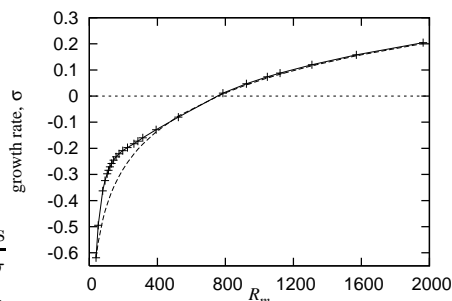


FIG. 2: The growth (or decay) rate of the r.m.s. magnetic field versus the magnetic Reynolds number for a flow shown in Fig. 1 with $\text{Re} \approx 16$; note that $\sigma = 0$ for $R_m = R_{m,\text{cr}} \approx 753$. The dashed curve is an asymptotic fit as discussed in the text.

where V is total volume, as obtained numerically via Fourier transform of \mathbf{u} given by Eq. (2) with the input from Eq. (3). Although the flow is not random, it exhibits Lagrangian chaos [13, 14], which facilitates the dynamo action. The flow is stationary on average, so we expect that the mean magnetic energy density will vary exponentially in time, $\langle B^2 \rangle^{1/2} \propto e^{\sigma t}$, with the growth (or decay) rate σ depending on R_m and the kinetic energy spectrum [7]. Meanwhile, the spatial form of the magnetic field is expected to remain statistically stationary.

We solve the induction equation (1) in a unit cubic periodic box discretized in 128^3 grid cubes. We begin with a periodic, seed magnetic field with energy distributed equally at 5 different scales in the box. After a small number of timesteps, the 5-peaked magnetic energy spectrum smooths out to become a horizontal flat spectrum. Figure 2 shows σ , measured in terms of the turnover time at the smallest velocity scale, $2\pi/\omega_\eta$. Dynamo action is initiated at $R_{m,\text{cr}} \approx 753$ for the Kolmogorov spectrum, $s = -5/3$. The data were obtained by changing R_m (or η) without changing the flow. Thus, the effective magnetic Prandtl number $P_m = R_m/\text{Re}$ varies together with R_m . Also plotted (dashed curve) is the

asymptotic behavior suggested for $R_m \gg 1$ in ref. [7]: $\sigma \approx \alpha(\mathcal{U}/\mathcal{L}) \ln(R_m/R_{m,\text{cr}})$, where \mathcal{U} and \mathcal{L} are a representative speed and length respectively and α is a constant of order unity; [7] obtain $\alpha \approx 2/3$ for $\mathcal{U} = u_0$, $\mathcal{L} = 2\pi/k_0$. A very good fit to our results is achieved for a similar value $\alpha \approx 0.6$ (or ≈ 0.2 if the dissipation scale is used). The accuracy of this fit for $R_m > R_{m,\text{cr}}$ is over 96%. Magnetic structures at the largest values of R_m and k considered here may be only marginally resolved with the resolution 128^3 (cf. ref. [12]) but note that the size of our computational box is unity rather than 2π . However, the systematic behavior of the growth rate and magnetic spectrum at the largest values of R_m and k indicate that the numerical resolution is sufficient; we carefully checked for other signs of insufficient resolution in our results but none were found.

The energy spectrum $M(k)$ of the growing magnetic field (defined similarly to $E(k)$) for $R_m \approx 2000$ is shown in Fig. 1 (dotted line), where it exhibits a range with $M(k) \propto k^{3/2}$ expected for a small-scale dynamo with a single-scale random flow [5]. As we discuss below, our model also reproduces all other known features of the small-scale dynamo that we have tested.

Asymptotic solutions of the induction equation for $R_m \gg 1$ relevant to the small-scale dynamo have been interpreted as indicating that magnetic field is mostly concentrated into filaments of thickness $l_\eta = l_0 R_m^{-1/2}$ (for single-scale flows) [6] or $l_\eta = l_0 R_m^{-2/(1-s)}$ for flows with kinetic energy spectral index s [7, 8, 9]. However, more recent numerical simulations appeared to display magnetic sheets and ribbons [10, 11, 12]. The latter conclusion was based on the visual inspection of magnetic isosurfaces and application of heuristic morphology indicators. Here we apply mathematically justified morphology quantifiers, based on the Minkowski functionals [18], to isosurfaces of magnetic energy density such as those shown in Fig. 3. This tool has previously been applied to galaxy distribution and cosmological structure formation [19, 20, 21].

The morphology of structures in three dimensions can be fully quantified using the four Minkowski functionals:

$$\begin{aligned} V_0 &= \iiint dV, & V_1 &= \frac{1}{6} \iint dS, \\ V_2 &= \frac{1}{6\pi} \iint (\kappa_1 + \kappa_2) dS, & V_3 &= \frac{1}{4\pi} \iint \kappa_1 \kappa_2 dS, \end{aligned} \quad (4)$$

where integration is over the volume and surface of the structures, respectively, and κ_1 and κ_2 are the principal curvatures of the surface. The Minkowski functionals can be used to calculate the typical thickness, width and length of the structures, as $T = V_0/2V_1$, $W = 2V_1/\pi V_2$, and $L = 3V_2/4V_3$, respectively. Then, useful dimensionless measures of ‘planarity’ P , and ‘filamentarity’ F [19] can be defined as $P = (W - T)/(W + T)$, $F = (L - W)/(L + W)$. In idealized cases and for convex

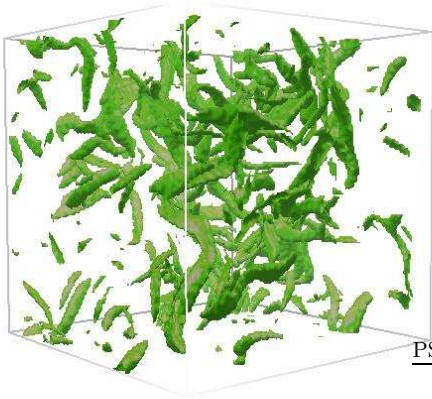


FIG. 3: (color online) The $B^2 = 3\langle B^2 \rangle$ isosurfaces of magnetic energy density for the flow of Fig. 1 with $R_m = 1570$.

surfaces, values of P and F lie between zero and unity. For example, an infinitely thin pancake has $(P, F) = (1, 0)$, a perfect filament has $(P, F) = (0, 1)$, whereas $(P, F) = (0, 0)$ for a sphere. A $B^2 = 1.5\langle B^2 \rangle$ isosurface of the initial magnetic field has $(P, F) = (0.094, 0.14)$. Some other examples are shown on the right-hand side of Fig. 4. We note that the unit cube has $T = 3/4$, $W = 2/\pi$, $L = 1/2$, thus these measures are not necessarily such that $T < W < L$. Deviations from this ordering are relatively rare for random fields studied here, yet to avoid confusion we introduce the notation $l_1 = \min(T, W, L)$, $l_2 = \text{med}(T, W, L)$ and $l_3 = \max(T, W, L)$.

As shown in Fig. 4, F increases faster than P with R_m , so the magnetic structures produced by the small-scale dynamo are better described as filaments, especially at the larger values of R_m . Remarkably, similar velocity field structures are not filamentary since the wave vectors in Eq. (2) have no preferred direction, hence the velocity field at small scales is nearly isotropic. Correspondingly, the isosurfaces of \mathbf{u}^2 have negligible planarity and filamentarity. The isosurface of vorticity $\boldsymbol{\Omega}$ with $\Omega^2 = 4\langle \Omega^2 \rangle$ has $(P, F) = (0.18, 0.11)$; similarly the isosurface of the total strain ($S^2 = S_{ij}S_{ij}$) with $S^2 = 4.5\langle S^2 \rangle$ has $(P, F) = (0.11, 0.16)$. Thus, the morphology of the magnetic field is controlled by the nature of the dynamo action rather than by immediate features of the velocity field. Isosurfaces of the electric current density $\mathbf{J} = \nabla \times \mathbf{B}$ are ribbon-like, with $(P, F) = (0.57, 0.82)$ at a level $J^2 = 4\langle J^2 \rangle$ for $R_m = 1570$.

Using the Minkowski functionals, we can also reliably measure the characteristic length scales of magnetic structures and explore their scalings with R_m and s . In Fig. 5, we display l_1 against R_m at two instants in time for the flow with $s = -5/3$ shown in Fig 1. Whilst the behavior for $R_m \ll R_{m,cr}$ shows variations in time, we observe for $R_m \gtrsim 200$ a time-independent scaling of the thickness of magnetic structures: $l_1 = 2\pi/k_\eta \sim R_m^{-3/4}$. This scaling, obtained in ref. [7] for a flow δ -correlated in

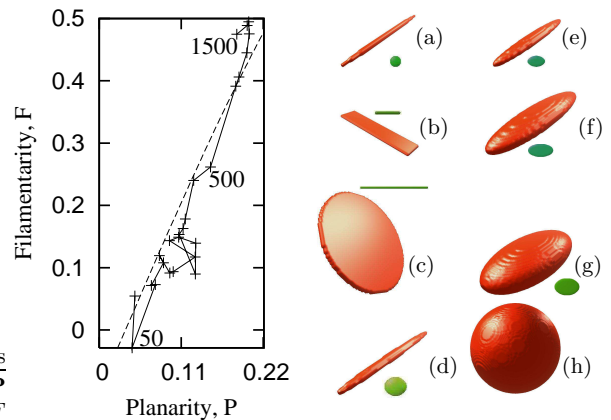


FIG. 4: (color online) The route taken by magnetic structures through the (P, F) -plane as R_m increases, averaged for each R_m between eight isosurfaces ranging from $B^2 = 1.5\langle B^2 \rangle$ to $B^2 = 5\langle B^2 \rangle$ in steps of $0.5\langle B^2 \rangle$; in this range the magnetic structures depend only weakly on the choice of isosurface. Three data points are labelled with their values of R_m . The dashed line is the estimates of Eq. (6). The objects on the right, from a filament to a sphere, are shown for reference: $(P, F) =$ (a) (0.096, 0.81); (b) (0.66, 0.23); (c) (0.66, 0.12); (d) (0.25, 0.66); (e) (0.18, 0.43); (f) (0.14, 0.23); (g) (0.087, 0.073) and (h) (0.0036, -0.0047). The cross section (in green) is also displayed for each object, except for (h) where it is circular.

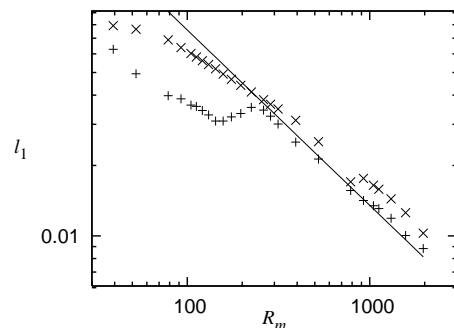


FIG. 5: Average values of the thickness l_1 of the isosurface structures against R_m at two instants in time for the flow of Fig. 1. Data marked 'x' ('+') are results attained when the smallest eddies have made 25 (50) revolutions. The solid straight line has a gradient of $-3/4$.

time (see also ref. [8, 9]) follows from the balance of the induction and diffusion terms in the induction equation [22]: a flow with energy spectrum $E(k) \propto k^s$ yields

$$l_1 \simeq l_0 R_m^{-2/(1-s)}. \quad (5)$$

The reason for the R_m -dependence of this scale is akin to that of the magnetic diffusion length, or the skin-depth.

Figure 6 shows the characteristic width l_2 and length l_3 of the magnetic structures against R_m . For $R_m \gtrsim 200$ we observe another time-independent scaling, $l_2 \sim R_m^{-0.55}$. This distinct behavior of the width of magnetic structures has not been obtained in earlier analytical or

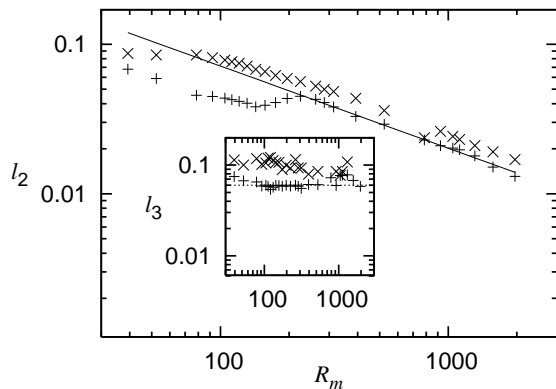


FIG. 6: As in Fig. 5, but for the width l_2 (main frame) and length l_3 (inset). The solid straight line in the main plot has a gradient of -0.55 .

numerical studies of the small-scale dynamo. The simultaneous decrease of l_2 and l_1 , coupled with the approximately R_m -independent behavior of l_3 (Fig. 6 inset) supports the notion that the magnetic structures become filamentary as R_m increases (see Fig. 4). Indeed, using $l_1 \sim 2.4R_m^{-0.75}$, $l_2 \sim 0.9R_m^{-0.55}$ and $l_3 \sim 0.05R_m^0$ in the definitions of P and F , we can estimate, for $s = -5/3$,

$$P \sim 1 - 2[1 + \frac{3}{8}R_m^{0.2}]^{-1}, \quad F \sim 1 - 2[1 + \frac{1}{18}R_m^{0.55}]^{-1}, \quad (6)$$

so that $F > P$ for $R_m \gtrsim 200$. These relations are shown by the dashed line in Fig. 4.

To investigate how the scaling laws identified via the Minkowski functionals compare with those inferred from other measures, we calculated the inverse ‘integral scale’ of the magnetic field, $2\pi/l_I = \int kM(k)dk / \int M(k)dk$. We found that l_I follows a scaling of $R_m^{-0.42}$, which understandably differs from the scalings of l_1 , l_2 and l_3 . The scale l_I is a poor measure of the dimension of anisotropic magnetic structures such as filaments. We note that the above scaling of l_I is maintained for *all* subcritical and supercritical values of R_m , unlike the results of Figs. 5 and 6 which display well-defined, time-independent scalings only for $R_m \gtrsim 200$. We have verified that the scaling (5) emerges for $s = -5/3, -2, -3$. On the contrary, $l_2 \sim R_m^{-0.55}$ independently of s . Asymptotic solutions [7] suggest that the small-scale dynamo (with $\text{Pr}_m < 1$) is only possible for $s < -3/2$. Our results show that, for high effective Pr_m , the dynamo action is possible for $s = -1$ as well, although a scaling different from (5) is exhibited. In this context, we propose that the nature of the asymptotic solution, rather than the possibility of a dynamo, is different at $s = -1$ from that at $s < -3/2$. We also tested the proxy dimensions of ref. [23] but these do not show physically justifiable scalings.

The scaling of l_1 with R_m has been obtained [7, 8, 9] for flows with $\text{Pr}_m = R_m/\text{Re} \lesssim 1$, where the maximum of the magnetic spectrum occurs in the inertial range of turbulence. With the effective Re defined above, our

simulations have an effective $\text{Pr}_m > 1$. We cannot introduce a true Re because we do not solve the Navier-Stokes equation and therefore the kinematic viscosity is not defined in our model. The reason why scalings expected for $\text{Pr}_m \lesssim 1$ occur in our model which appears to have $\text{Pr}_m > 1$ remains unclear.

In conclusion, we have shown that velocity fields of the form (2) are able to initiate the small-scale dynamo. This model flow reproduces many properties of turbulence and thus offers a convenient tool to study dynamos in multi-scale, well controlled flows. A quantitative, mathematically justifiable description of the morphology of magnetic structures based on the Minkowski functionals indicates that, at least at the kinematic stage, magnetic field is concentrated into filaments rather than sheets or ribbons. We have confirmed that the characteristic thickness of magnetic structures scales with the magnetic Reynolds number as given in Eq. (5) for the energy spectrum slope of s , whereas the width varies as $R_m^{-0.55}$ independently of s , and the length is independent of R_m .

We acknowledge useful discussions with S. Tobias and K. Subramanian. This work was supported by the EPSRC grant PB/KH/037026987 and the Leverhulme Trust grant F/00 125/N.

-
- [1] R. Beck, A. Brandenburg, D. Moss, A. Shukurov, and D. Sokoloff, *Ann. Rev. Astron. Astrophys.* **34**, 155 (1996).
 - [2] A. A. Schekochihin et al., *Astrophys. J.* **629**, 139 (2005).
 - [3] K. Subramanian, A. Shukurov, and N. E. L. Haugen, *MNRAS* **366**, 1437 (2006).
 - [4] T. A. Enßlin and C. Vogt, *Astron. Astrophys.* **453**, 447 (2006).
 - [5] A. P. Kazantsev, *Soviet Physics JETP* **26**, 1031 (1968).
 - [6] Y. B. Zeldovich, A. A. Ruzmaikin, and D. D. Sokoloff, *Magnetic Fields in Astrophysics* (Gordon & Breach, N.Y., 1983).
 - [7] I. Rogachevskii and N. Kleeorin, *Phys. Rev. E* **56**, 417 (1997).
 - [8] D. Vincenzi, *J. Stat. Phys.* **106**, 1073 (2002).
 - [9] S. Boldyrev and F. Cattaneo, *Phys. Rev. Lett.* **92**, 144501 (2004).
 - [10] A. A. Schekochihin et al., *Astrophys. J.* **625**, L115 (2005).
 - [11] A. Brandenburg and K. Subramanian, *Phys. Rep.* **417**, 1 (2005).
 - [12] P. D. Mininni, A. G. Pouquet, and D. C. Montgomery, *Phys. Rev. Lett.* **97**, 244503 (2006).
 - [13] N. A. Malik and J. C. Vassilicos, *Phys. Fluids* **11**, 1572 (1999).
 - [14] J. C. H. Fung and J. C. Vassilicos, *Phys. Rev. E* **57**, 1677 (1998).
 - [15] R. Monchaux et al., *Phys. Rev. Lett.* **98**, 044502 (2007).
 - [16] N. E. L. Haugen, A. Brandenburg, and W. Dobler, *Phys. Rev. E* **70**, 016308 (2004).
 - [17] A. A. Schekochihin et al., *Astrophys. J.* **612**, 276 (2004).
 - [18] M. A. Armstrong, *Basic Topology* (Springer, 1983).
 - [19] V. Sahni, B. S. Sathyaprakash, and S. F. Shandarin, *Astrophys. J.* **495**, L5 (1998).

- [20] J. Schmalzing and T. Buchert, *Astrophys. J.* **482**, L1 (1997).
- [21] J. Schmalzing *et al.*, *Astrophys. J.* **526**, 568 (1999).
- [22] K. Subramanian, *Phys. Rev. Lett.* **83**, 2957 (1999).
- [23] A. A. Schekochihin *et al.*, *Astrophys. J.* **612**, 276 (2004).